Article No. jmbi.1999.2921 available online at http://www.idealibrary.com on IDEAL® J. Mol. Biol. (1999) 290, 797–809

JMB

Role of the Salt-bridge between Switch-1 and Switch-2 of *Dictyostelium* Myosin

Marcus Furch[1], Setsuko Fujita-Becker[1], Michael A. Geeves[2], Kenneth C. Holmes[1] and Dietmar J. Manstein[1]*

[1]*Max-Planck-Institut für Medizinische Forschung Jahnstr. 29 D-69120 Heidelberg, Germany*

[2]*Max-Planck-Institut für Molekulare Physiologie Postfach 102664 D-44026 Dortmund, Germany*

**Corresponding author*

Motifs N2 and N3, also referred to as switch-1 and switch-2, form part of the active site of molecular motors such as myosins and kinesins. In the case of myosin, N3 is thought to act as a γ-phosphate sensor and moves almost 6 Å relative to N2 during the catalysed turnover of ATP, opening and closing the active site surrounding the γ-phosphate. The closed form seems to be necessary for hydrolysis and is stabilised by the formation of a salt-bridge between an arginine residue in N2 and a glutamate residue in N3. We examined the role of this salt-bridge in *Dictyostelium discoideum* myosin. Myosin motor domains with mutations E459R or R238E, that block salt-bridge formation, show defects in nucleotide-binding, reduced rates of ATP hydrolysis and a tenfold reduction in actin affinity. Inversion of the salt-bridge in double-mutant M765-IS eliminates most of the defects observed for the single mutants. With the exception of a 2,500-fold higher K_M value for ATP, the double-mutant displayed enzymatic and functional properties very similar to those of the wild-type protein. Our results reveal that, independent of its orientation, the salt-bridge is required to support efficient ATP hydrolysis, normal communication between different functional regions of the myosin head, and motor function.

Keywords: kinetics; recombinant protein; molecular motor; ATP hydrolysis; actomyosin

Introduction

Myosins and kinesins share a common fold surrounding the nucleotide. This structural core of both motor proteins consists of seven β-strands and six α-helices and contains a group of conserved sequence motifs, termed N1-N4, that contact the nucleotide and show sequence similarity to the G1-G4 motifs of G-proteins (Vale, 1996). Based on these similarities, it was suggested that G-proteins and motors use similar strategies for undergoing conformational changes between NTP and NDP states (Smith & Rayment, 1996a). The functional transitions that occur following nucleotide hydrolysis are best understood for G-proteins, whose structures have been solved in the GTP and GDP conformation (Pai *et al.*, 1990; Schlichting *et al.*, 1990; Tong *et al.*, 1991; Sprang, 1997). These structures show that the flexible G2 and G3 loop regions at the rear of the nucleotide binding pocket act as γ-phosphate sensors. The loops move ~4 Å towards each other when GTP is bound and move away from each other when GDP occupies the binding pocket. As these movements act mechanistically as a switch, G2 and G3 are frequently referred to as switch-1 and switch-2. The

Present address: M.A. Geeves, Department of Biosciences, University of Kent, Canterbury CT2 7NJ, Kent, UK.

Abbreviations used: acto·M, complex of actin and myosin head fragment; DTT, 1.4-dithiothreitol; EDTA, ethylenediaminetetraacetic acid; EGTA, ethyleneglycol-bis-(2-aminoethylether)-*N*,*N*,*N*′,*N*′-tetraacetic acid, k_{cat}, maximum turnover rate in the presence of actin; K_{app}, apparent K_M for actin; K_{ATP}, K_M for ATP; HMM, heavy meromyosin; LDH, lactate dehydrogenase; mantADP, 2′(3′)-*O*-(*N*-methylanthranilloyl)adenosine 5′-diphosphate; MHF, myosin head fragment; MHC, myosin heavy chain; *mhc*A, gene encoding MHC; ORF, open reading frame; PEP, phosphoenolpyruvate; pyr-actin, pyrene-labeled actin; PK, pyruvate kinase; S1, subfragment 1 of myosin; TNP-ATP, 2′-(or-3′)-*O*-(trinitrophenyl) adenosine 5′-triphosphate.

E-mail address of the corresponding author: manstein@mpimf-heidelberg.mpg.de

0022-2836/99/280797–13 $30.00/0

N2 and N3 residues in motor proteins also appear to function as γ-phosphate sensors. In myosin, switch-2 undergoes a large conformational change while switch-1 undergoes only minor conformational changes. The equilibrium between the open and closed forms seems to be delicately poised, since both forms are observed with ADP·BeF_3 as ATP analogue (Fisher *et al*., 1995; Smith & Rayment, 1996b; Dominguez *et al*., 1998; our unpublished results). Nevertheless, the presence of the γ-phosphate or a phosphate analogue seems to be needed for the formation of the closed form. The closed-cleft structure observed for the ADP·VO_4 form appears to be favoured by the formation of hydrogen bonds between the N3-glycine residue (G457) with the γ-phosphate. The closed form is further stabilised by the formation of a salt-bridge between the N2-arginine (R238) and N3-glutamate (E459) residues (Figure 1(a)), which is similar to the switch-1-switch-2 salt-bridge described for EF-Tu and kinesin (Berchtold *et al*., 1993; Kozielski *et al*., 1997; Sack *et al*., 1997). The importance of the N3 glycine and glutamate for myosin ATPase activity was established by mutational analysis (Ruppel & Spudich, 1996; Friedman *et al*., 1998). Opening of the cleft destroys the γ-phosphate-binding pocket, as can be seen in the crystal structure of nucleotide-free S1 prepared from chicken pectoralis muscle (Rayment *et al*., 1993b). In the open form, the switch-2 region is pulled away from the nucleotide-binding pocket and the N3-glycine and N3-glutamate residues are moved out of the active site. Therefore, hydrolysis can only proceed when the cleft shuts.

Here, we performed site-directed mutagenesis of *Dicytostelium discoideum* myosin II to dissect the effects of changing separately the salt-bridge residues R238 and E459 from those resulting from the loss of the salt-bridge. A similar study was reported recently by Onishi and co-workers who examined the role of the salt-bridge in chicken smooth muscle myosin by producing mutants R247E, E470R and R247E/E470R in the baculovirus expression system (Onishi *et al*., 1998). Their study showed that, whether in the normal or in the inverted orientation, the salt-bridge is necessary for ATP hydrolysis. However, when the salt-bridge is in the inverted direction it does not support actin activation, a finding which suggest that the protein is unable to function as a molecular motor. We produced three versions of *D. discoideum* myosin motor domain construct M765 (Furch *et al*., 1998) with mutations R238E, E459R and R238E/E459R (Figure 1(b)), respectively. These mutant motor domain constructs will be referred to as R238E, E459R and M765-IS, with ''IS'' referring to inverted salt-bridge. The more efficient production of protein in *D. discoideum* allowed a wider ranging set of assays to be performed, and a detailed study of the interaction of the mutant motor domains with actin and nucleotide is presented. Additionally, a full-length myosin version of the double-mutant was produced. This myosin-IS construct was used to confirm that the mutant protein can act as a functional motor *in vivo* and *in vitro*. This result was not expected on the basis of the study by Onishi *et al*. (1998) using smooth muscle myosin mutants.

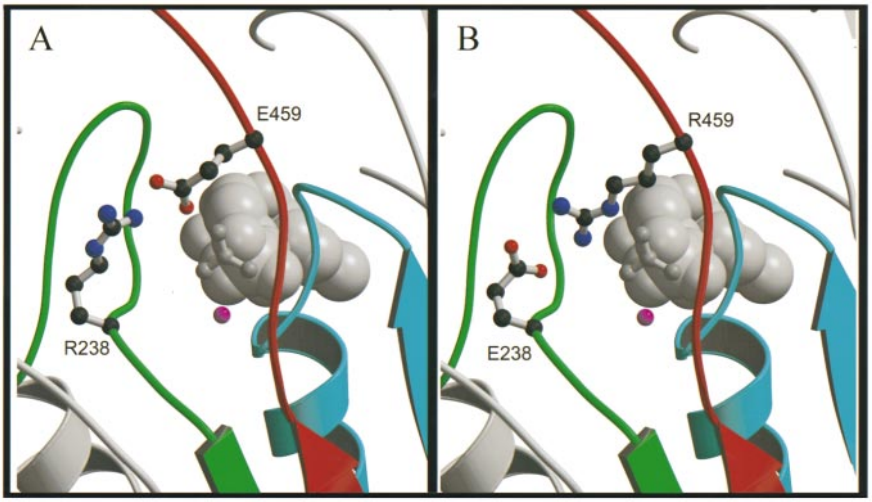

Figure 1. Ribbon representation of the γ-phosphate pocket of *D. discoideum* myosin II. (a) The salt-bridge formed by residues R238 and E459 in the closed form of *D. discoideum* myosin II complexed with ADP and BeF_3 is shown (I. Schlichting, F.J. Kull, D.J.M. & K.C.H., unpublished results). (b) Model of the γ-phosphate pocket with the salt-bridge in the inverted orientation. ADP and BeF_3 are shown in grey. ADP as spheres and BeF_3 in ball-and-stick representation in front. The purple sphere corresponds to the magnesium ion. Loops surrounding the nucleotide are coloured green for switch-I, red for switch-II, and cyan for the P-loop. The Figure was produced with the programs Bobscript (Esnouf, 1997) and Raster3D (Merritt & Bacon, 1997).

Results

Binding of ATP to myosin head fragments

Binding and hydrolysis of ATP by *D. discoideum* myosin head fragments was analysed in terms of the seven-step model described by Bagshaw *et al*. (1974) shown in Scheme 1, where M refers to myosin head fragment and T, D, and P_i to ATP, ADP and phosphate, respectively. The asterisks refer to different conformations as detected by intrinsic protein fluorescence. Step 1 corresponds to the formation of a binary collision complex. Following the ATP-induced conformational change (step 2), ATP is hydrolysed in step 3. Step 4 is the slowest step in the scheme and corresponds to a conformational change that precedes phosphate release in step 5. ADP is released in a relatively slow two-step reaction, steps 6 and 7, that is similar to a reversal of the two-step association of ATP. The interaction of ATP and skeletal muscle myosin S1 is associated with two changes in the intrinsic protein fluorescence: an increase on ATP binding is followed by a further increase as ATP is hydrolysed. Accordingly, a smaller change in amplitude is observed upon binding of ADP to skeletal muscle S1. In the case of *D. discoideum* myosin II, ADP binding does not lead to an increase in intrinsic protein fluorescence. It was therefore concluded that the fluorescence change observed upon ATP binding to the *D. discoideum* protein is only associated with the hydrolysis step (Ritchie *et al*., 1993).

$$M + T \underset{k_{-1}}{\overset{k_{+1}}{\rightleftharpoons}} M \cdot T \underset{k_{-2}}{\overset{k_{+2}}{\rightleftharpoons}} M^* \cdot T \underset{k_{-3}}{\overset{k_{+3}}{\rightleftharpoons}} M^{**} \cdot D \cdot P_i \underset{k_{-4}}{\overset{k_{+4}}{\rightleftharpoons}}$$

$$M^* \cdot D \cdot P_i \underset{k_{-5}}{\overset{k_{+5}}{\rightleftharpoons}} P_i + M^* \cdot D \underset{k_{-6}}{\overset{k_{+6}}{\rightleftharpoons}} M \cdot D \underset{k_{-7}}{\overset{k_{+7}}{\rightleftharpoons}} M + D$$

Scheme 1.

The addition of excess ATP increased the intrinsic protein fluorescence intensity by 22 % in the case of M765 and by 3 % for M765-IS. There was no measurable change of protein fluorescence following addition of excess ATP to R238E and E459R. The transient fluorescence increase observed with M765 and M765-IS is well described by a single exponential function and the observed rate constants were linearly dependent on the concentration of ATP at low ATP concentrations. In the range from 5 to 25 μM ATP, the slope of the plot of k_{obs} against ATP concentration defined the rate constant of ATP binding (Figure 2). Second-order binding constants (K_1k_{+2}) of 8.6×10^5 M^{-1} s^{-1} for M765 and of 0.6×10^5 M^{-1} s^{-1} for M765-IS were obtained (see Table 1). At higher ATP concentrations (>1 mM), k_{obs} was no longer linearly dependent upon [ATP] and the data were well described by a hyperbola ($k_{obs} = k_{max}$ [ATP]/([ATP] + $K_{0.5}$)). The maximum rate of the fluorescence change k_{max} was 30 s^{-1} for M765 and approximately 100 s^{-1} for M765-IS. For myosin subfragment-1 (S1) it was proposed that k_{max} corresponds to the rate of the ATP hydrolysis step ($k_{+3} + k_{-3}$) (Marston & Taylor, 1980).

Binding of fluorescent nucleotides to myosin head fragments

Since R238E and E459R failed to show any change in intrinsic protein fluorescence when mixed with ATP, we used fluorescent nucleotides to measure binding. Hiratsuka synthesised a range of nucleotides with fluorescent groups attached to the ribose moiety, which exhibit catalytic properties similar to those of the physiological nucleotides (Hiratsuka & Uchida, 1973; Hiratsuka, 1983). ATP analogues equipped with either a trinitrophenyl (TNP-ATP) or an N-methylanthraniloyl group (mantATP) are widely used to study the interaction between ATP and myosin (Hiratsuka, 1976; Cremo *et al*., 1990; Woodward *et al*., 1995). Binding of TNP-ATP or mantATP resulted in a change in fluorescence for all of the mutant myosin head fragments when the fluorophore was excited at 406 nm or at 360 nm, respectively. The fluorescence changes observed with TNP-ATP were small for all myosin head fragments, with amplitudes between 2 and 10 % (data not shown). Addition of 10 μM mantATP to 0.5 μM myosin head fragments produced increases in N-methylanthraniloyl fluorescence of 21 %, 11 %, and 53 % for R238E, E459R, and M765-IS, respectively, compared to a value of 70 % for wild-type. Figure 3(a) shows transients with a best fit to a single-expo-

Table 1. Summary of rate constants for the interaction of nucleotides with myosin head fragments

Nucleotide	Rate constant	M765	R238E	E459R	M765-IS
ATP	K_1k_{+2}[a]	8.6×10^5	na	na	0.6×10^5
	$k_{+3}+k_{-3}$[b]	30 ± 1	na	na	103 ± 10
mantATP	K_1k_{+2}[a]	11.3×10^5	0.3×10^5	3.3×10^5	9.7×10^5
TNP-ATP	K_1k_{+2}[a]	9.8×10^5	0.4×10^5	2.0×10^5	1.1×10^5
mantADP	k_{-6}/K_7[a]	10.2×10^5	0.4×10^5	3.9×10^5	8.6×10^5
	k_{+6}[b]	1.6	0.0054	0.18	1.5
	$K_{D\ (calc.)}$[c]	1.6	0.1	0.4	1.7

[a] M^{-1} s^{-1}.
[b] s^{-1}.
[c] μM.

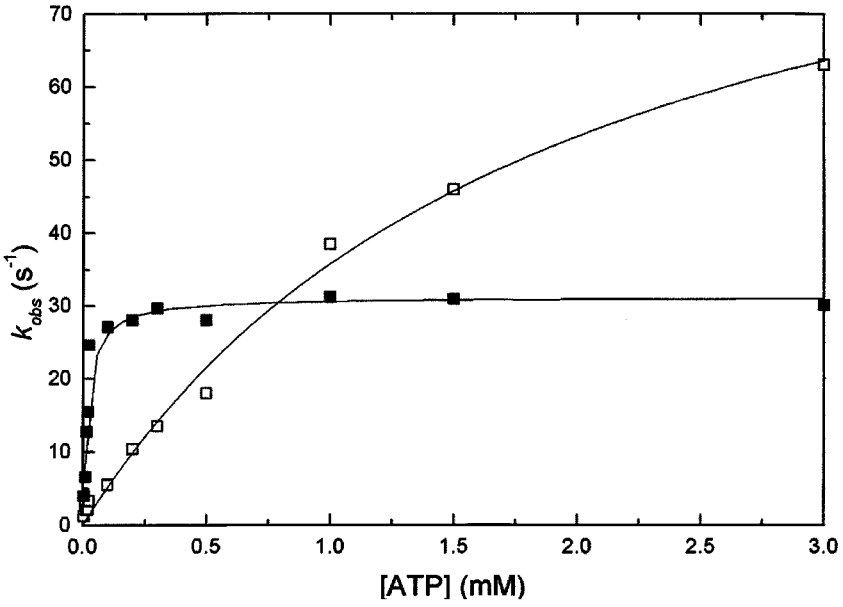

Figure 2. Rate of ATP binding and hydrolysis by M765 and M765-IS. MHF (0.5 μM) was mixed with an excess of ATP in a rapid mixing stopped-flow fluorometer and the time-dependent changes in the intrinsic protein fluorescence recorded. The fluorescence increased and could be described by an exponential function ($(F_t - F_\infty) = (F_o - F_\infty)\exp(-k_{obs}nt)$) and k_{obs} is plotted against [ATP]. The data set for each MHF was well described by a hyperbola, although the model for rabbit S1 does not predict a hyperbolic dependence of k_{obs} on [ATP]. The profiles are due to a change in the rate limiting step; with the ATP binding kinetics (K_1k_{+2}) limiting at low [ATP] and the cleavage step ($k_{+3} + k_{-3}$) limiting at high [ATP]. The least-squares fit to hyperbolae are shown superimposed and k_{max}, the predicted k_{obs} at infinite [ATP] and $K_{0.5}$, the concentration of ATP when $k_{obs} = k_{max}/2$ were: M765-IS (□), $k_{max} = 103\ s^{-1}$, $K_{0.5} = 2$ mM; M765 (■), $k_{max} = 30\ s^{-1}$, $K_{0.5} = 17$ μM. At low concentrations in the range from 0 to 25 μM the data fit a straight line. The slopes of these lines define the apparent second-order rate constants of ATP binding (see Table 1). In each case the intercept was not significantly different from zero. Conditions: 20 mM Mops, 5 mM $MgCl_2$, and 100 mM KCl (pH 7.0) at 20 °C.

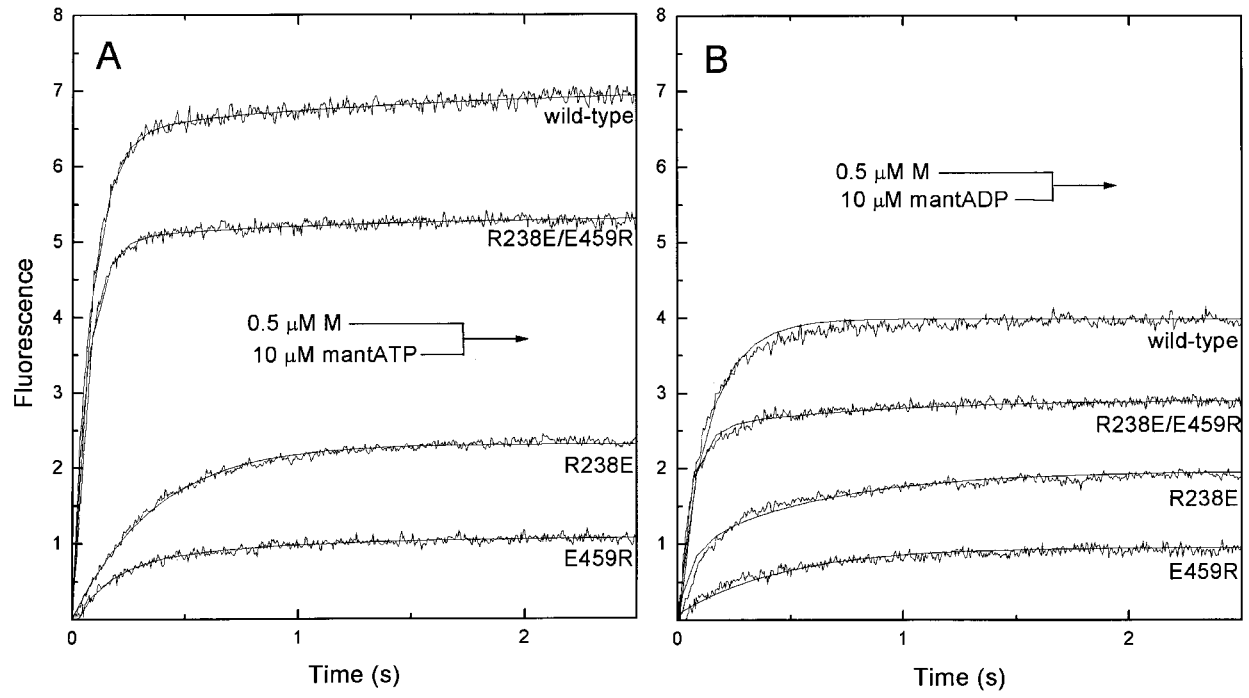

Figure 3. Binding of mant-nucleotides to myosin head fragments. (a) Stopped-flow records obtained upon mixing 10 μM mantATP with 0.5 μM mutant myosin head fragments. Mant-fluorescence was excited at 366 nm and detected after passing through a KV 389 nm cut-off filter. The continuous lines are the best fits to a single exponential with $k_{obs} = 12.1\ s^{-1}$ amp. + 70 % for M765, $k_{obs} = 0.7\ s^{-1}$ amp. +21 % for R238E, $k_{obs} = 1.6\ s^{-1}$ amp. +11 % for E459R, and $k_{obs} = 7.8\ s^{-1}$ amp. +53 % for M765-IS, respectively. (b) Stopped-flow records obtained upon mixing 10 μM mantADP with 0.5 μM M765 ($k_{obs} = 10.2\ s^{-1}$ amp. + 41 %), R238E ($k_{obs} = 0.9\ s^{-1}$ amp. + 21 %), E459R ($k_{obs} = 1.9\ s^{-1}$ amp. + 10 %), and M765-IS ($k_{obs} = 9.0\ s^{-1}$ amp. + 29 %), respectively. Conditions: 20 mM Mops, 5 mM $MgCl_2$, and 100 mM KCl (pH 7.0), at 20 °C.

nential superimposed. The observed rate constants were linearly dependent on either TNP-ATP or mantATP concentration, in the concentration range from 5 to 25 μM. Similar second-order rate constants of approximately $\times 10^6$ $M^{-1}s^{-1}$ were obtained for ATP and both analogues in the case of M765 (Table 1). The second-order rate constant for mantATP binding to M765-IS gave a similar value, while TNP-ATP and ATP binding was ten- to 18-fold slower with M765-IS. In comparison to M765, either ATP analogue bound ~30-fold more slowly to R238E and three- to fivefold more slowly to E459R. Since the excitation spectrum of mantATP closely overlaps the emission spectrum of tryptophan residues, mantATP, when bound to myosin head fragments, can also be excited at 295 nm (Millar & Geeves, 1988; Ritchie *et al*., 1993). In the case of M765 and M765-IS, identical fluorescence time-courses were observed when mantATP fluorescence was excited directly and indirectly. However, no energy transfer from tryptophan to mantATP was seen for R238E and E549R.

The reaction for mantADP binding was studied over the concentration range from 5 to 25 μM, and the second-order rate constants for mantADP binding (k_{-6}/K_7) are summarised in Table 1. Nearly identical rates of mantADP binding were observed for M765 and M765-IS. Figure 3(b) shows transients observed on adding 10 μM mantADP to 0.5 μM myosin head fragments. Changes in signal intensity similar to those observed with mantATP were observed upon the addition of mantADP to R238E (21 %) and E459R (10 %). However, mantADP gave smaller fluorescence changes with M765 (41 % *versus* 70 %) and M765-IS (29 % *versus* 53 %) than seen for mantATP. This observation is consistent with the assumption that the fluorescence increase that follows the addition of mantATP to S1 monitors two distinct steps: a fluorescence increase on mantATP binding followed by a further increase concomitant with a conformational change that precedes mantATP hydrolysis (Woodward *et al*., 1991).

Rate of ADP release from myosin head fragments

The ADP dissociation rate constant was measured by displacing mantADP from mutant constructs with excess ATP. The rate of the ensuing decrease in fluorescence is determined by the rate of mantADP dissociation. Figure 4 shows the reaction observed on adding 200 μM ATP to 0.5 μM M·mantADP. The transient decrease in mant-fluorescence was fitted to a single exponential. The value of k_{obs} gives the rate of mantADP dissociation k_{+6} as 1.6 s^{-1} for M765, 0.0054 s^{-1} for R238E, 0.18 s^{-1} for E459R, and 1.5 s^{-1} for M765-IS, respectively (Table 1). The ratio of $k_{+6}/(k_{-6}/K_7)$ defines the affinity for mantADP (K_D) giving values of 1.6 μM, 0.1 μM, 0.4 μM, and 1.7 μM for wild-type, R238E, E459R, and M765-IS, respectively.

Binding of nucleotides to acto·M

The experiments in the presence of actin could be analysed in terms of models developed by Millar & Geeves (1983) and Siemankowski & White (1984), as previously demonstrated in a series of studies with *D. discoideum* myosin head fragments (Ritchie *et al*., 1993; Kurzawa *et al*., 1997). In this scheme, A and M represent actin and myosin head fragments, respectively.

$$A \cdot M + ATP \overset{\mathbf{K_1}}{\rightleftharpoons} A \cdot M \cdot ATP \xrightarrow{\mathbf{k_{+2}}} A + M \cdot ATP \longrightarrow$$

Scheme 2.

A first step in which ATP binds rapidly and reversibly to acto·M ($\mathbf{K_1}$) is followed by a rate-limiting isomerization ($\mathbf{k_{+2}}$) of the complex leading to rapid dissociation of actin. Thus, the observed rate constant for ATP-induced dissociation of the acto·M complex is defined at low ATP concentrations by $k_{obs} = [ATP]\,\mathbf{K_1 k_{+2}}$.

The rate of ATP-induced dissociation of acto·M was monitored by observing the fluorescence-increase of a pyrene label on actin that occurs following the addition of excess ATP. The observed rate was linearly related to the concentration of ATP up to 25 μM and yielded second-order rate constants of 2.5×10^5 M^{-1} s^{-1} for M765 and of 1.7×10^5 M^{-1} s^{-1} for M765-IS (Figure 5(a)). For the single point mutants, R238E and E459R, two- to eightfold faster values of 5.0×10^5 M^{-1} s^{-1} and 19.5×10^5 M^{-1} s^{-1} were determined, respectively. The amplitudes of the fluorescence signals were reduced to 39 % (R238E), 25 % (E459R), and 84 % (M765-IS) of the wild-type level.

In the presence of ADP there is competition between the two nucleotides for binding to the acto·M complex. Assuming that ADP is in rapid equilibrium with acto·M, then for a fixed ATP concentration k_{obs} is given by the equation $k_{obs} = k_0/(1 + [ADP]/\mathbf{K_{AD}})$ where k_0 is the observed rate constant in the absence of ADP. The affinity of ADP for the acto· M complex can therefore be determined from the competitive inhibition of ATP-induced dissociation of pyr-acto·M. Transients were recorded on adding 100 μM ATP to 0.5 μM pyr-acto·M in the presence of up to 3.2 mM ADP. The records were monophasic for all constructs. For M765, the observed rate of ATP-induced dissociation of the acto·M complex was 28.5 s^{-1} in the absence of ADP and decreased to 2.0 s^{-1} at the highest ADP concentration used. Upon addition of 3.2 mM ADP to the mutant constructs, k_{obs} decreased from 38 s^{-1} to 6.5 s^{-1} for R238E, from 124 s^{-1} to 4.7 s^{-1} for E459R, and from 27 s^{-1} to 4.7 s^{-1} for M765-IS (Table 2). A plot of the observed rate constants against the ADP concentrations was fitted to the equation as shown in Figure 5(b). Dissociation constants $\mathbf{K_{AD}}$ of approximately 250 μM were determined for the three

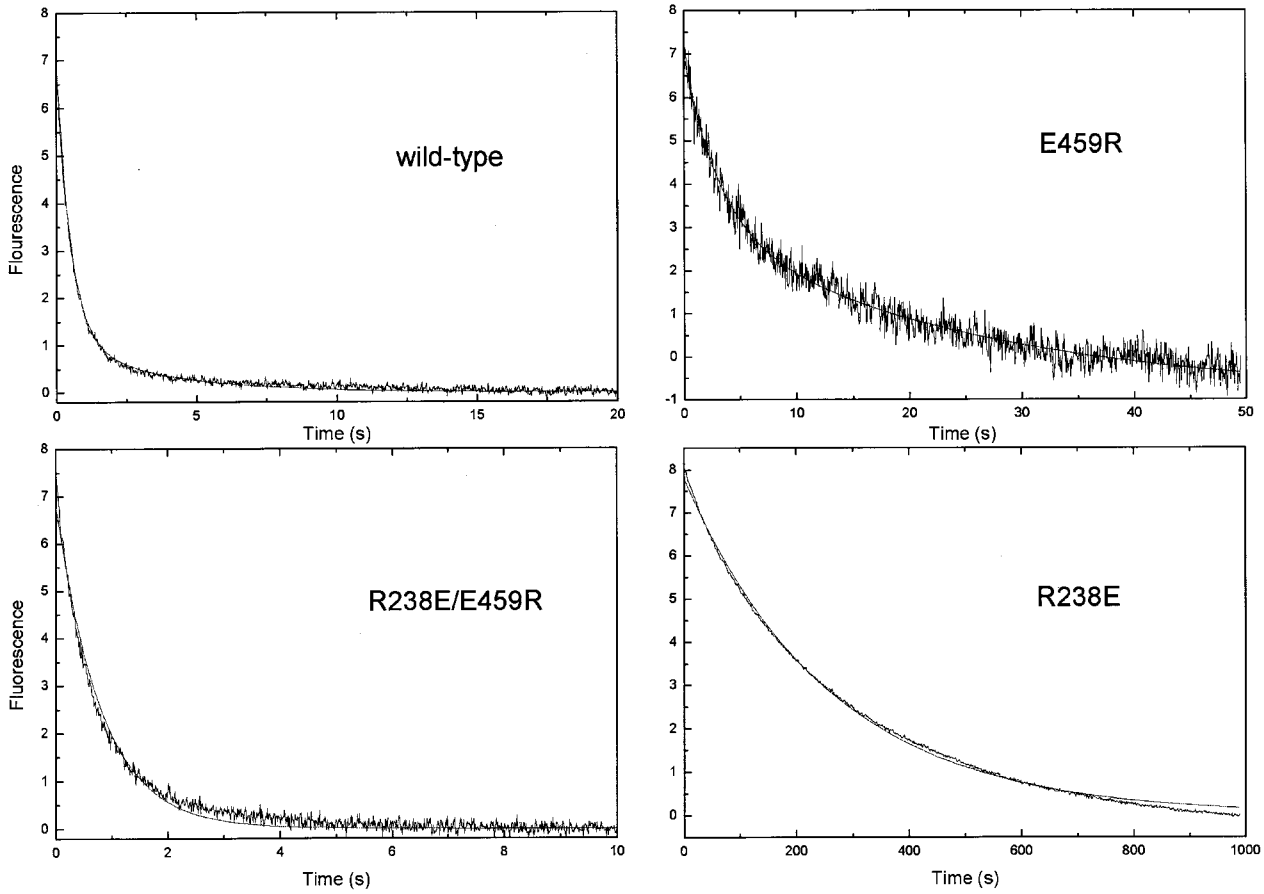

Figure 4. The rate of ADP dissociation from myosin head fragments was measured by displacement of mantADP from a 0.5 μM M·mantADP complex by 200 μM ATP. The observed decrease in mant-fluorescence could be fitted to a single exponential where k_{obs} corresponds to k_{+6}/K_7. Values are listed in Table 1. Conditions: 20 mM MOPS, 5 mM $MgCl_2$, and 100 mM KCl (pH 7.0) at 20 °C.

mutant acto·M complexes and of 58 μM for acto·M765.

Actin binding and dissociation

The rate of the formation of the acto·M complex ($\mathbf{k_{+A}}$) was measured by mixing excess pyr-actin with 0.25 μM myosin head fragment and monitoring the decrease of pyrene-fluorescence as actin binds. All transients were described by a single exponential, and the observed rate constants were linearly dependent on the actin concentration up to 5 μM (data not shown). The second-order binding rate constants given by the slopes of the resulting secondary plots were essentially identical for all constructs. However, large changes were observed in the amplitude of the fluorescence signal (see below).

The dissociation rate constant for actin was determined directly by displacing 0.5 μM pyr-actin from the pyr-acto·M complex by a 40-fold excess of unlabeled actin (Figure 6). The increase in pyrene fluorescence was fitted to a single exponential. The observed rate for the process corresponds to $\mathbf{k_{-A}}$, and gave rate constants of 0.048 s^{-1}, 0.066 s^{-1}, and 0.003 s^{-1} for R238E, E459R, and M765-IS, respectively, compared to 0.006 s^{-1} for M765. The amplitudes were 13 % (R238E), 44 % (E459R), and 71 % (M761-IS), relative to those observed with M765. The dissociation equilibrium constant ($\mathbf{K_A}$) for actin binding to different mutant constructs, calculated from the ratios of $\mathbf{k_{-A}}$ and $\mathbf{k_{+A}}$, are listed in Table 3.

Table 2. Summary of rate constants for the interaction of nucleotides with pyr-acto·M complexes

Rate constant				
	M765	R238E	E459R	M765-IS
$\mathbf{K_1k_{+2}}$ ($M^{-1}s^{-1}$)	2.5×10^5	5.0×10^5	19.5×10^5	1.7×10^5
$\mathbf{K_{AD}}$ (μM)	58 ± 3	190 ± 18	290 ± 50	235 ± 15

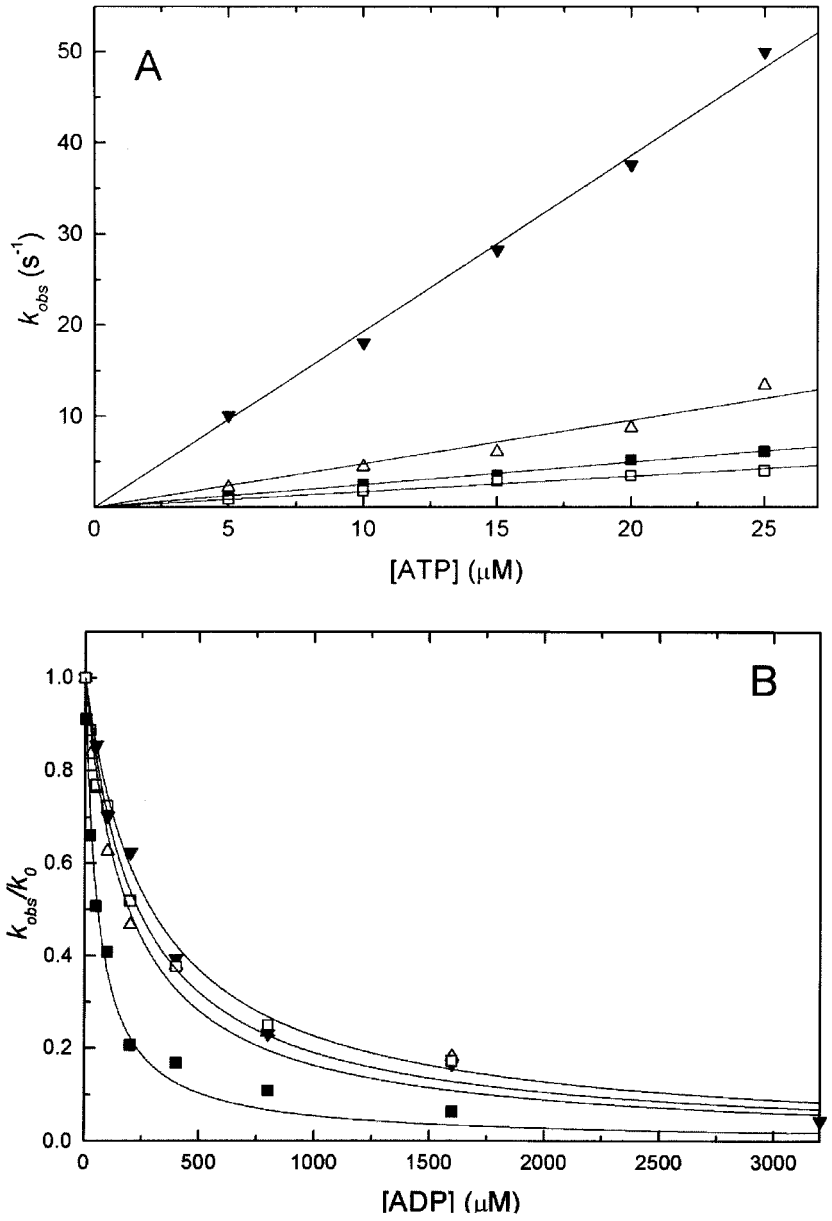

Figure 5. Interaction of the actin-bound protein with nucleotides. (a) ATP-induced dissociation of pyr-acto·M. At low ATP concentrations k_{obs} was linearly dependent upon [ATP] and the slopes define the second-order binding $\mathbf{K_1k_{+2}}$. In each case the intercept was not significantly different from zero. The symbols correspond to the following *D. discoideum* myosin fragment mutants: M765 (■), R238E (△), E459R (▼), and M765-IS (□). (b) ADP inhibition of ATP-induced dissociation of pyr-acto·M. Dependence of the rate of the observed process on ADP concentration. Plot of k_{obs}/k_0 *versus* ADP concentration. The dissociation constants of the ADP complexes were determined by fitting a plot according to the following equation: $k_{obs}/k_0 = 1/(1 + [ADP]/\mathbf{K_{AD}})$; k_0 = observed rate constant in the absence of ADP. The fits gave values of 58(±3) μM (M765/■), 190(±20) μM (R238E/△), 290(±50) μM (E459R/▼), and 235(±15) μM (M765-IS/□). Conditions: 20 mM Mops, 5 mM $MgCl_2$, and 100 mM KCl (pH 7.0) at 20 °C.

Steady-state rate of ATP hydrolysis

At an ionic strength of $I = 0.06$ M and in the presence of 0.5 mM Mg^{2+}-ATP, M765 and M765-IS showed basal ATPase activities of 0.08 s^{-1} and 0.01 s^{-1}, respectively. The transient ATP binding experiments indicated a 14-fold slower on-rate (K_1k_{+2}) for M765-IS in comparison to the wild-type value. Therefore, we performed the steady-state measurements over a wider range of ATP concentrations (1 μM to 10 mM) to examine the effect on basal ATPase activity. Figure 7 shows the [ATP]-dependence of the ATPase reaction for M765 and M765-IS. The K_M of myosin head fragments for ATP ($K_{M(ATP)}$) and the maximum of the basal ATPase were calculated from fitting the data to the Michaelis-Menten equation, which yielded $K_{M(ATP)}$ values of <2 μM, ~5 mM, and ~20 mM for M765, M765-IS and E459R, respectively. The basal ATPase activity at saturating ATP concentration

Table 3. Summary of rate constants for acto·M association and dissociation

Rate constant	M765	R238E	E459R	M765-IS
$\mathbf{k_{+A}}$ ($M^{-1}s^{-1}$)	1.34×10^6	1.19×10^6	1.46×10^6	1.37×10^6
$\mathbf{k_{-A}}$ (s^{-1})	0.006	0.048	0.066	0.003
$\mathbf{K_A}$ (calc) (nM)	4.5	40	41	2.3

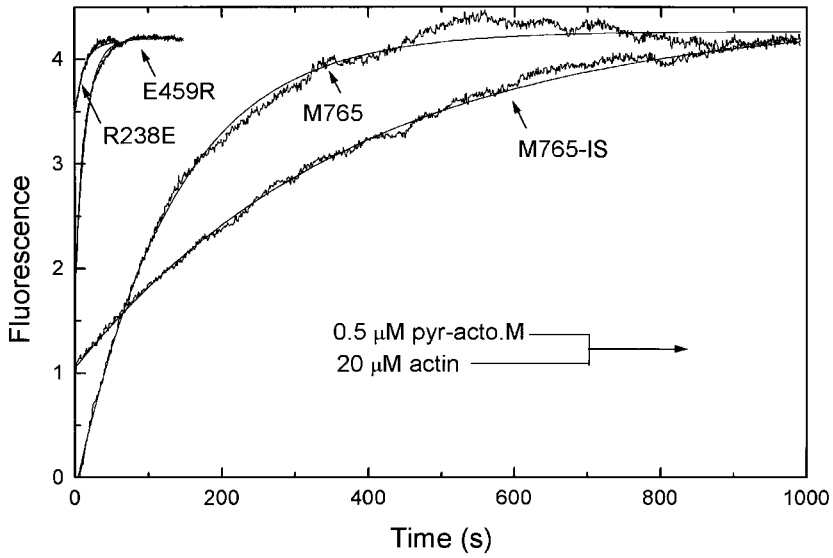

Figure 6. Stopped-flow records of the increase in pyrene fluorescence during the pyr-actin displacement of 0.5 μM of the pyr-acto·M complex with 20 μM unlabelled actin. The best fits to a single-exponential are superimposed with $k_{obs} = 0.048\ s^{-1}$, $0.066\ s^{-1}$, $0.003\ s^{-1}$, and $0.006\ s^{-1}$ for R238E, E459R, M765-IS, and M765, respectively.

was $0.08\ s^{-1}$ for M765 and M765-IS and $0.015\ s^{-1}$ for E459R. The basal ATPase activity of R238E did not increase with ATP concentration and had a value of $4 \times 10^{-4}\ s^{-1}$.

Addition of actin activated the ATPase activity of E459R and M765-IS, but not of R238E. In the presence of 20 μM rabbit skeletal muscle F-actin, steady-state ATPase rates increased to $0.55\ s^{-1}$ for M765, $0.09\ s^{-1}$ for E459R, and $0.31\ s^{-1}$ for M765-IS. The acto·M ATPase activity measured for the three constructs was independent of the ATP concentration in the observed range between 0.5 and 6 mM, but increased almost linearly with increasing actin concentration up to 80 μM, the highest concentration used. The data sets were fitted to straight lines and values for the apparent second-order rate constant of the reaction, k_{cat}/K_{app}, were obtained from the slopes. The resulting values were $0.25 \times 10^5\ M^{-1}\ s^{-1}$ for M765, $0.04 \times 10^5\ M^{-1}\ s^{-1}$ for E459R, and $0.15 \times 10^5\ M^{-1}\ s^{-1}$ for M765-IS. To determine if the decrease in k_{cat}/K_{app} is associated with a reduced affinity for actin or with a decrease in the maximum turnover rate, values for k_{cat} and K_{app} were analysed graphically using double-reciprocal plots. Values of $0.4\ s^{-1}$ (E459R), $2.1\ s^{-1}$ (M765-IS) and $2.8\ s^{-1}$ (M765) were obtained for k_{cat}. K_{app} was estimated as 130(±30) μM for all three constructs (Table 4).

Functional competence of myosin-IS

The functional competence of myosin-IS *in vivo* was analysed by testing the ability of cells pro-

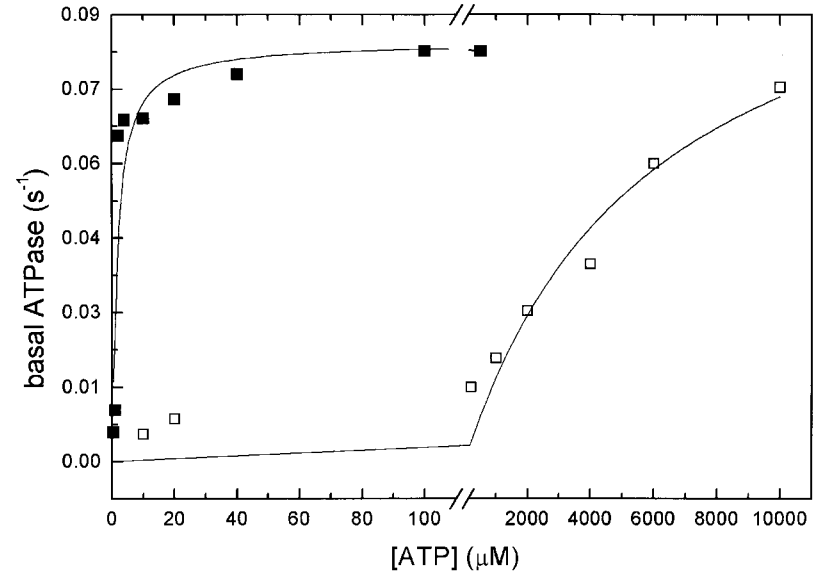

Figure 7. Dependence of the Mg^{2+}-ATPase on the ATP concentration in the absence of actin. The data are fitted to a hyperbola and gave values for $K_{M(ATP)}$ of 1.7 μM for M765 and 5 mM for M765-IS, respectively. The plateau values for both myosin head fragments were $0.08\ s^{-1}$. In addition to the components of the linked assay (0.2 mM NADH, 0.5 mM PEP, 0.02 mg/ml LDH, 0.05 mg/ml PK) the buffer contained 25 mM imidazole, 25 mM KCl, 10 mM $MgCl_2$, 0.5 mM 1.4-dithiothreitol, pH 7.4. Assays were performed in the presence of 400 nM to 10 mM Mg^{2+}-ATP.

Table 4. Summary of the steady-state parameters of the ATPase activities of myosin head fragments and their actin complexes

	Wild-type	R238E	E459R	R238E/E459R
Basal (s^{-1})[a]	0.08 ± 0.01	4 (±5)× 10^{-4}	0.015 ± 0.005	0.06 ± 0.002
$K_{M(ATP)}$ (μM)[b]	1.7 ± 0.5	n.a.	~20 × 10^3	5(±1)× 10^3
k_{cat}/K_{app} ($M^{-1}s^{-1}$)[c]	0.25 × 10^5	n.a.	0.03 × 10^5	0.15 × 10^5
k_{cat} (s^{-1})[c]	2.8 ± 0.5	n.a.	0.4 ± 0.1	2.1 ± 0.6
K_{app} (μM)[c]	120 ± 20	n.a.	130 ± 20	130 ± 20

[a] Measurements were carried out in 25 mM imidazole, 25 mM KCl, 4 mM $MgCl_2$, and 6 mM ATP (pH 7.4).
[b] $K_{M(ATP)}$ was determined from Figure 7. The buffer contained between 0.4 μM and 10 mM Mg^{2+} − ATP.
[c] k_{cat} and K_{app} were calculated by fitting the data to the Michaelis-Menten equation. All measurements were performed at 25 °C.

ducing myosin-IS to undergo cytokinesis and form fruiting bodies, processes that require functional myosin in *D. discoideum*. Unlike the parent *mhc*A$^-$ cells (Manstein *et al*., 1989), transformants producing myosin-IS are able to form fruiting bodies and grow in suspension culture with doubling times comparable to those of wild-type cells (Figure 8).

Analysis of myosin-IS in an *in vitro* movement assay (Kron & Spudich, 1986) showed that the mutant myosin moves actin filaments only 2.5-fold slower than native *D. discoideum* myosin. Sliding velocities of 0.4 μm s^{-1} and 1.0 μm s^{-1} were measured for myosin-IS and wild-type myosin, respectively.

Discussion

M765-IS and myosin-IS

Inversion of the salt-bridge-forming residues R238 and E459 leaves the kinetic and functional properties of the myosin motor largely unaffected. The affinity for actin ($\mathbf{K_A}$) and the second-order rate constant ($\mathbf{K_1k_{+2}}$) for the ATP-induced dissociation of acto·M are very similar for M765 and M765-IS. Addition of saturating concentrations of actin leads to a 34-fold activation of the ATPase activity of both M765 and M765-IS, resulting in k_{cat} values of 2.8(±0.5) s^{-1} and 2.1(±0.6) s^{-1}, respectively. The rates of mantATP binding, mantADP

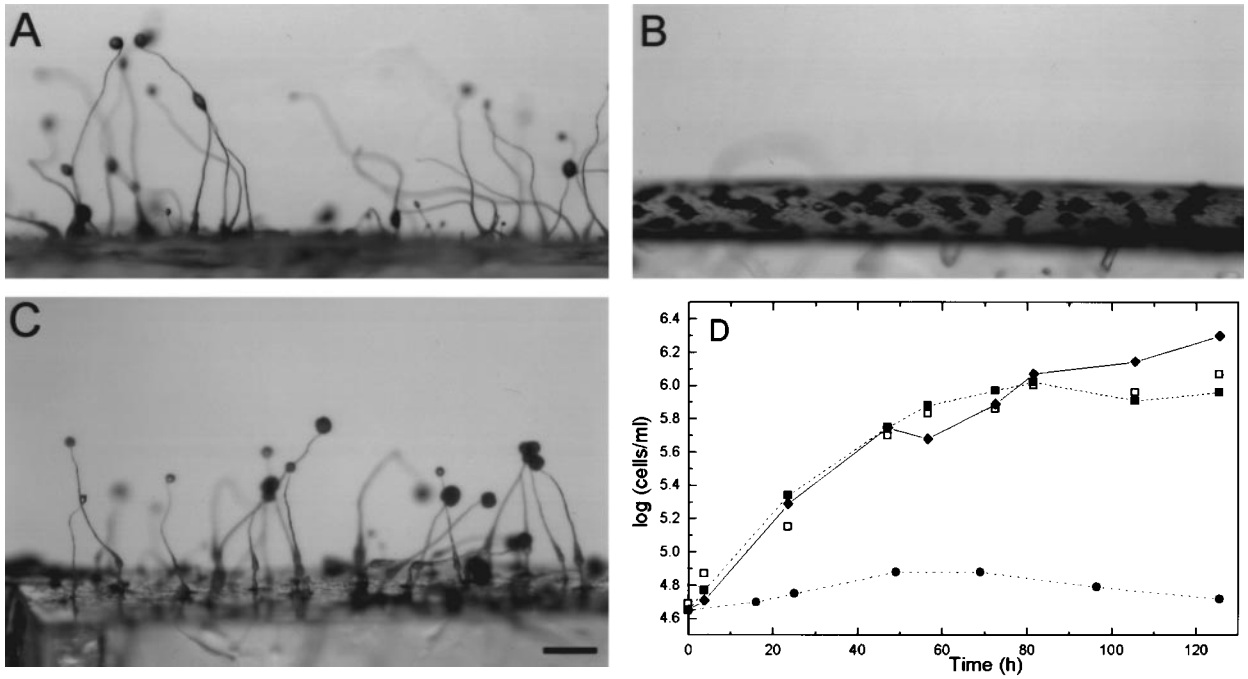

Figure 8. Functional complementation of *D. discoideum* myosin null cells. (a) Wild-type cells form fruiting bodies consisting of a long stalk bearing an unwalled, globose spore mass. (b) Myosin-depleted cells are not able to form fruiting bodies and viable spores. (c) Transformation of myosin null cells with a vector for the expression of myosin-IS rescued fruiting body formation and the production of viable spores. The scale bar represents 1 mm. (d) Growth in suspension. Myosin null-cells producing myosin-IS (□) grow at the same rate as wild-type cells (◆) and myosin null-cells producing a recombinant form of the native myosin (■). The parental myosin null cells are not able to grow in suspension (●).

binding, and mantADP dissociation are similar, and single-turnover rates differ by less than two-fold between M765 and M765-IS (data not shown). The slow rate of ATP binding to M765-IS and the resulting low affinity for ATP, reflected in a $K_{M(ATP)}$ value of 5 mM, constitute the only major defects of M765-IS. The low affinity for ATP is most likely a product of the charge change at R238E which will result in repulsion of the negatively charged ATP. Onishi *et al*. (1998) suggested that chicken smooth muscle myosin with the salt-bridge inversion retains a normal P_i-burst, a normal level of intrinsic fluorescence enhancement, and displays normal intrinsic ATPase activity in the presence of 0.5 mM ATP.

While the differences in the fluorescence sensitivity of the *D. discoideum* and smooth muscle myosin constructs may simply result from the fact that the smooth muscle myosin motor domain has three additional tryptophan residues (W31,W546 and W625), the remaining differences are more difficult to interpret.

At saturating concentrations of ATP (>10 mM), the rate of the ATP cleavage step ($k_{+3} + k_{-3}$) is even faster for M765-IS (103 s^{-1}) than for M765 (30 s^{-1}) and the basal ATPase activity of M765-IS is restored reaching wild-type level (0.08 s^{-1}). Since M765-IS displays almost normal interactions with ATP and ADP in the presence of actin and since millimolar concentrations of ATP are present in *D. discoideum* cells, myosin-IS is expected to function normally *in vivo*. This assumption was confirmed by transforming *D. discoideum* myosin-null cells with the mutant gene. Transformants producing myosin-IS appear normal for cytokinesis, development and sporogenesis. The *in vitro* motility data reflect the similarities in the kinetic behaviour of double-mutant and wild-type and give additional confirmation of the mechanical integrity of myosin-IS.

R238E and E459R

The findings that R238E and E459R displayed reduced intrinsic ATPase activity and that E459R, but not R238E, shows normal levels of actin activation are in good agreement with previous studies (Shimada *et al*., 1997; Sasaki *et al*., 1998; Onishi *et al*., 1998). The rates of binding fluorescently labelled nucleotides to E459R are reduced three- to fourfold compared to M765 but for R238E by more than 20-fold. This supports the suggestion that the charge change in R238E is significant in inhibiting nucleotide binding. The rates of mantADP and mantATP binding to M765-IS are close to the normal values, suggesting that the second charge change (E459R), the ability to form the salt-bridge, or a combination of both effects rescues normal nucleotide binding. For the single point mutation E459R, the effects on the rates of nucleotide binding are quite mild and in a related mutation, E459V, we showed that the rate of mantATP binding was even slower than for E459R. Yet, the affinity of ATP for E459V remains very high at 3×10^{-10} M (Friedman *et al*., 1998). Thus the loss of the salt-bridge itself does not induce a major change in ATP affinity. However, the lack of a P_i-burst observed for the smooth muscle myosin mutant (Onishi *et al*., 1998) and the results of acid quench experiments performed with E459V (Friedman *et al*., 1998) suggest that for E459R, too, k_{cat} is given by the ATP cleavage step.

Interaction of the mutant proteins with actin

Remarkable aspects of this analysis are the way and extent to which alterations of the salt-bridge forming residues affect the interaction with actin and coupling between the actin and nucleotide binding sites. We have previously shown that the interaction of *D. discoideum* myosin II with actin can be analysed in terms of the three-state model described for skeletal muscle myosin (Geeves & Conibear, 1995):

$$A + M(N) \overset{K_0}{\rightleftharpoons} \underset{\text{Collision complex}}{A \sim M(\cdot N)} \overset{K_1}{\rightleftharpoons} \underset{\text{A-State}}{A - M(\cdot N)} \overset{K_2}{\rightleftharpoons} \underset{\text{R-State}}{A \cdot M(\cdot N)}$$

Scheme 3.

The kinetic data show that the affinity of constructs R238E and E459R for actin is tenfold reduced and in the case of M765-IS is twofold increased. The mutations affect only $\mathbf{k_{-A}}$ which corresponds to $\mathbf{k_{-1}/(1 + K_2)}$, while $\mathbf{k_{+A}}$ which corresponds to $\mathbf{K_0 k_{+1}}$ is unchanged (see Table 3).

This result indicates that the formation of the initial collision complex and the weakly bound, attached or A-state is little affected by mutations that prevent formation of the salt-bridge and stabilisation of the closed form. Therefore, A-state formation appears to be dominated by local changes in the actomyosin interface rather then the status of the nucleotide pocket. Compared to M765, addition of R238E, E459R and M765-IS to pyrene-actin reduced the amplitude of the pyrene-fluorescence signal only by 13, 44 and 71%, respectively. As fluorescence quenching is thought to occur when myosin undergoes the conformational change from the A-state to the strongly bound, rigor or R-state (Furch *et al*., 1998), a reduced level of fluorescence quenching could result from a shift in equilibrium between A to R-state in favour of the A-state. However, this interpretation cannot be correct as M765-IS has increased affinity for actin and any significant shift in the equilibrium between A and R-states should lead to a much larger reduction in affinity than the tenfold decrease observed for R238E and E459R. Changes in specific fluorescence signals are notoriously difficult to correlate with structural changes because they are extremely sensitive to small local perturbations. However, the reduced amplitude of the pyrene-fluorescence does clearly indicate changes in the actin binding site of the mutant myosins that

are likely to result from the formation of a perturbed R-state. This interpretation is consistent with the mutations having only an effect on k_{-A} and crystallographic evidence that suggests that, while the A-state can be formed with any myosin-nucleotide complex, the formation of the R-state requires the outward movement of switch-2 and opening of the backdoor (Holmes, 1998). Finally, the tenfold faster dissociation rate constants of the single mutants suggest that closing of the backdoor is not a prerequisite for dissociation from actin.

Actin also has a strong effect on the interaction of the mutant myosins with nucleotides. In contrast to the situation in the absence of actin, all mutants showed normal or increased rates of ATP binding. The addition of actin had a much stronger effect on the mutants' affinity for ADP, as the ratio of $\mathbf{K_{AD}}/K_D$ is close to 36 for M765 compared to values of 1900, 725 and 138 for R238E, E459R and M765-IS, respectively. This indicates that the salt-bridge influences both the nucleotide and actin binding sites of myosin and forms an essential part of the communication pathway between the different functional regions of the myosin motor.

In summary, our results show that inversion of the salt-bridge forming residues in *D. discoideum* myosin II leaves not only intrinsic functions but also the interaction with actin and the mechanical properties of the myosin motor largely unaffected. Inversion of the salt-bridge between residues R238 and E459 of *D. discoideum* myosin II produces a functional myosin motor with almost normal properties. This result was not expected on the basis of an earlier study where smooth muscle myosin mutants were used to examine the role of the salt-bridge (Onishi *et al*., 1998). In future studies, it will be important to examine the reason for the different behaviour of the mutant myosins.

Materials and Methods

Construction, expression and purification of recombinant myosin motors

All subcloning was done following standard procedures (Sambrook *et al*., 1989). A recombinant plasmid pDH20, which was derived from the extrachromosomal vector pDXA-3H has been described (Furch *et al*., 1998). pDH20 contains sequence coding for the first 765 residues of the *D. discoideum mhc*A gene fused to a C-terminal His_8-tag. M765 was expressed under the control of the *D. discoideum* actin 15 promoter. Mutant constructs were generated by the method described by Braman *et al* (1996). The following mutagenic primers were used (nucleotide changes corresponding to a single amino acid substitution are underlined): M765(R238E), 5′-GCCAAAACCACCCGTAACAACAATTCATCTGAATT CGGTAAAT TCATTG and 5′-CAATGAATTTACCGA ATTCAGATGAATTGTTGTTACGGGTGGTT TTGGC; M765(E459R), 5′-GGTGTTTTGGATATTTCAGGTTTTCG AATTTTCAAAG TCAATTCATTCG and 5′-CGAATGA ATTGACTTTGAAAATTCGAAAACCTGAAATA TCCA AAACACC. The new plasmids were designated pDH20(R238E) and pDH20(E459R), respectively. Next, the primer pair that was used before to generated pDH20(R238E) was used in a second PCR in combination with pDH20(E459R) which resulted in the creation of the vector pDH20(R238E/E459R) encoding for M765-IS. Additionally, a construct for the preparation of a full-length myosin bearing the R238E/E459R mutation was made by using pDH4 which contains the complete *D. discoideum mhc*A coding sequence. Removing the *Sac*I-*Bst*XI fragment from pDH4 and replacing it with the *Sac*I-*Bst*XI fragment from pDH20(R238E/E459R) resulted in the generation of pFL(R238E/E459R). Loss of an additional *Nsi*I site in pDH4 facilitated screening of the transformants using diagnostic *Nsi*I/*Nco*I digests. Each DNA construct was confirmed by sequencing to ensure that the desired mutation had been introduced.

D. discoideum transformants were grown at 21 °C in HL-5C (Furch *et al*., 1998). Transformants were selected and screened for the production of the recombinant myosin motor domains as described (Manstein *et al*., 1995). The His-tagged motor domains were purified as described by Manstein & Hunt (1995). The purified protein could be stored at −80 °C for several months without apparent loss of enzymatic activity. Purification of full-length wild-type and mutated myosin-IS was performed using a rapid purification protocol that involves sequential rounds of myosin assembly and disassembly as described by Uyeda & Spudich (1993).

Rabbit F-actin was isolated by the method described by Lehrer & Kewar (1972) with minor modifications (Furch *et al*., 1998). Actin was labelled with pyrene at Cys374 (pyr-actin) as described (Criddle *et al*., 1985). The 2′(3′)-*O*-(*N*-methylanthranilloyl) derivatives of ADP and ATP (mantADP, mantATP) were prepared described by Hiratsuka (1983). The 2′-(or-3′)-*O*-(trinitrophenyl) adenosine 5′-triphosphate (TNP-ATP) was purchased from Molecular Probes.

Stopped-flow experiments and direct functional assays

Stopped-flow experiments for transient kinetics were performed at 20 °C in 20 mM MOPS, 5 mM $MgCl_2$, and 100 mM KCl (pH 7.0) with a Hi-tech Scientific SF61 or SF-61DX stopped-flow spectrophotometer using a 75W Xe/Hg lamp and a monochromator for wavelength selection. For tryptophan fluorescence, excitation was at 295 nm, with emission through a WG 320 cut-off filter. Pyrene and mant fluorescence was excited at 365 nm and emission monitored after passing through a KV 389 nm cut-off filter. TNP fluorescence was excited at 406 nm and detected after passage through an OG450 cut-off filter (all cut-off filters, Schott, Mainz). Data were stored and analysed using software provided by Hi-tech. Transients shown are the average of three to five consecutive shots of the stopped-flow machine. The experiments were repeated with proteins from at least one different preparation. All concentrations refer to the concentration of the reactants after mixing in the stopped-flow observation cell.

The experiments were analysed in terms of the models shown in the Schemes. In these schemes a notation is used that distinguishes between the constants in the presence and absence of actin by using bold ($\mathbf{k_{+1}}$, $\mathbf{K_1}$) versus italics type (k_{+1}, K_1); subscript A and D refer to actin ($\mathbf{K_A}$) and ADP (K_D), respectively.

Steady-state ATPase rates were measured using a linked enzyme assay and analysed as described previously (Furch *et al*., 1998). In the presence of actin, assays were performed at Mg^{2+}-ATP concentrations in

the range from 0.5-6 mM. Basal ATPase was measured in the presence of 1 μM to 10 mM Mg^{2+}-ATP.

The *in vitro* motility assay was performed at 20 °C as described (Anson *et al*., 1996). Synchronous morphological differentiation was induced by starvation on MMC agar (20 mM Mes (pH 6.8), 2 mM $MgCl_2$, 0.2 mM $CaCl_2$, 2% (w/v) Difco Bacto agar). Structures from various stages of development were visualised using an Olympus B061 microscope and a Sony SSC-M370CE video camera. A Hamamatsu Argus-20 was used for contrast enhancement and transfer of images to a Macintosh 9500.

Acknowledgements

M.F and S.F.-B. contributed equally to this work.

We thank S. Zimmermann for expert technical assistance and the generation of expression vectors for the mutant constructs; G. Helmig and N. Adamek for preparation of actin and pyr-actin; J. Wray for critical reading of the manuscript and discussions; R.S. Goody and K.C. Holmes for continual support and encouragement. The work was supported by the Max Planck Society and by grant MA 1081/5-1 to D.J.M. from the DFG.

References

Anson, M. (1992). Temperature dependence and Arrhenius activation energy of F-actin velocity generated *in vitro* by skeletal myosin. *J. Mol. Biol.* **224**, 1029-1038.

Bagshaw, C. R., Eccleston, J. F., Eckstein, F., Goody, R. S., Gutfreund, H. & Trentham, D. R. (1974). The magnesium ion-dependent adenosine triphosphatase of myosin. Two-step processes of adenosine triphosphate association and adenosine diphosphate dissociation. *Biochem. J.* **141**, 351-364.

Berchtold, H., Reshetnikova, L., Reiser, C. O., Schirmer, N. K., Sprinzl, M. & Hilgenfeld, R. (1993). Crystal structure of active elongation factor Tu reveals major domain rearrangements. *Nature,* **365**, 126-132.

Braman, J., Papworth, C. & Greener, A. (1996). Site-directed mutagenesis using double-stranded plasmid DNA templates. *Methods Mol. Biol,* **7**, 31-44.

Cremo, C. R., Neuron, J. M. & Yount, R. G. (1990). Interaction of myosin subfragment 1 with fluorescent ribose-modified nucleotides. A comparison of vanadate trapping and SH1-SH2 cross-linking. *Biochemistry,* **29**, 3309-3319.

Criddle, A. H., Geeves, M. A. & Jeffrries, T. (1985). The use of actin labelled with N-(1-pyrenyl) iodoacetamide to study the interaction of actin with myosin subfragments and troponin/tropomyosin. *Biochem. J.* **232**, 343-349.

Dominguez, R., Freyzon, Y., Trybus, K. M. & Cohen, C. (1998). Crystal structure of a vertebrate smooth muscle myosin motor domain and its complex with the essential light chain - visualization of the pre-power stroke state. *Cell,* **94**, 559-571.

Esnouf, R. M. (1997). An extensively modified version of MolScript that includes greatly enhanced coloring capabilities. *J. Mol. Graph.* **15**, 132-134.

Fisher, A. J., Smith, C. A., Thoden, J. B., Smith, R., Sutoh, K., Holden, H. M. & Rayment, I. (1995). X-ray structure of the myosin motor domain of *Dictyostelium discoideum* complex with MgADP· BeF_x and MgADP· AlF_4^-. *Biochemistry,* **34**, 8960-8972.

Friedman, A. L., Geeves, M. A., Manstein, D. J. & Spudich, J. A. (1998). Kinetic characterization of myosin head fragments with long-lived myosin-ATP states. *Biochemistry,* **37**, 9679-9687.

Furch, M., Geeves, M. A. & Manstein, D. J. (1998). Modulation of actin affinity and actomyosin adenosine-triphosphatase by charge changes in the myosin motor domain. *Biochemistry,* **37**, 6317-6326.

Geeves, M. A. & Conibear, P. B. (1995). The role of three-state docking of myosin S1 with actin in force generation. *Biophys. J.* **68**, 194S-201S.

Hiratsuka, T. (1976). Fluorescence properties of 2′ (or 3′)-O-(2,4,6-trinitrophenyl) adenosine 5′-triphosphate and its use in the study of binding to heavy meromyosin ATPase. *Biochim. Biophys. Acta,* **453**, 293-297.

Hiratsuka, T. (1983). New ribose-modified fluorescent analogs of adenine and guanine nucleotides available as substrates for various enzymes. *Biochim. Biophys. Acta,* **742**, 496-508.

Hiratsuka, T. & Uchida, K. (1973). Preparation and properties of 2′(or 3′)-O-(2,4,6-trinitrophenyl) adenosine 5′-triphosphate, an analog of adenosine-triphosphate. *Biochim. Biophys. Acta,* **320**, 635-647.

Holmes, K. C. (1998). A molecular model for muscle contraction. *Acta Crystallog. sect. A,* **54**, 789-797.

Kozielski, F., Sack, S., Marx, A., Thormahlen, M., Schonbrunn, E., Biou, V., Thompson, A., Mandelkow, E. M. & Mandelkow, E. (1997). The crystal structure of dimeric kinesin and implications for microtubule-dependent motility. *Cell,* **91**, 985-994.

Kron, S. J. & Spudich, J. A. (1986). Fluorescent actin filaments move on myosin fixed to a glass surface. *Proc. Natl Acad. Sci. USA,* **83**, 6272-6276.

Kurzawa, S. E., Manstein, D. J. & Geeves, M. A. (1997). *Dictyostelium discoideum* myosin II: characterization of functional myosin motor fragments. *Biochemistry,* **36**, 317-323.

Lehrer, S. S. & Kewar, G. (1972). Intrinsic fluorescence of actin. *Biochemistry,* **11**, 1211-1217.

Manstein, D. J. & Hunt, D. M. (1995). Overexpression of myosin motor domains in *Dictyostelium*: screening of transformants and purification of the affinity tagged protein. *J. Muscle Res. Cell Motil.* **16**, 325-332.

Manstein, D. J., Titus, M. A., De Lozanne, A. & Spudich, J. A. (1989). Gene replacement in *Dictyostelium*: generation of myosin null mutants. *EMBO J.* **8**, 923-932.

Manstein, D. J., Schuster, H.-P., Morandini, P. & Hunt, D. M. (1995). Cloning vectors for the production of proteins in *Dictyostelium discoideum*. *Gene,* **162**, 129-134.

Marston, S. B. & Taylor, E. W. (1980). Comparison of the myosin and actomyosin ATPase mechanisms of the four types of vertebrate muscles. *J. Mol. Biol.* **139**, 573-600.

Merrit, E. A. & Bacon, D. J. (1997). Raster3D: photorealistic molecular graphics. *Methods Enzymol.* **15**, 132-134.

Millar, N. C. & Geeves, M. A. (1983). The limiting rate of the ATP-mediated dissociation of actin from rabbit skeletal muscle myosin subfragment 1. *FEBS Letters,* **160**, 141-148.

Millar, N. C. & Geeves, M. A. (1988). Protein fluorescence changes associated with ATP and adenosine 5′-[γ-thio]triphosphate binding to skeletal muscle myosin subfragment 1 and actomyosin subfragment 1. *Biochem. J.* **249**, 735-743.

Onishi, H., Kojima, S., Katoh, K., Fujiwara, K., Martinez, H. M. & Morales, M. F. (1998). Functional transitions in myosin: formation of a critical salt-bridge and transmission of effect to the sensitive tryptophan. *Proc. Natl Acad. Sci. USA,* **95**, 6653-6658.

Pai, E. F., Krengel, U., Petsko, G. A., Goody, R. S., Kabsch, W. & Wittinghofer, A. (1990). Refined crystal structure of the triphosphate conformation of H-ras p21 at 1.35 A resolution: implications for the mechanism of GTP hydrolysis. *EMBO J.* **9**, 2351-2359.

Rayment, I., Holden, H. M., Whittaker, M., Yohn, C. B., Lorenz, M., Holmes, K. C. & Milligan, R. A. (1993a). Structure of the actin-myosin complex and its implications for muscle contraction. *Science,* **261**, 58-65.

Rayment, I., Rypniewski, W. R., Schmidt-Bäse, K., Smith, R., Tomchick, D. R., Benning, M. M., Winkelmann, D. A., Wesenberg, G. & Holden, H. M. (1993b). Three-dimensional structure of myosin subfragment-1: a molecular motor. *Science,* **261**, 50-58.

Ritchie, M. D., Geeves, M. A., Woodward, S. K. A. & Manstein, D. J. (1993). Kinetic characterization of a cytoplasmic myosin motor domain expressed in *Dictyostelium discoideum*. *Proc. Natl Acad. Sci. USA,* **90**, 8619-8623.

Ruppel, K. M. & Spudich, J. A. (1996). Structure-function analysis of the motor domain of myosin. *Annu. Rev. Cell Dev. Biol.* **12**, 543-573.

Sack, S., Muller, J., Marx, A., Thormahlen, M., Mandelkow, E. M., Brady, S. T. & Mandelkow, E. (1997). X-ray structure of motor and neck domains from rat brain kinesin. *Biochemistry,* **36**, 16155-16165.

Sambrook, J., Fritsch, E. F. & Maniatis, T. (1989). *Molecular Cloning: A Laboratory Manual*, Cold Spring Harbor Laboratory Press, Cold Spring Harbor, NY.

Sasaki, N., Shimada, T. & Sutoh, K. (1998). Mutational analysis of the switch II loop of *Dictyostelium* myosin II. *J. Biol. Chem.* **273**, 20334-20340.

Schlichting, I., Almo, S. C., Rapp, G., Wilson, K., Petratos, K., Lentfer, A., Wittinghofer, A., Kabsch, W., Pai, E. F. & Petsko, G. A. (1990). Time-resolved X-ray crystallographic study of the conformational change in Ha-Ras p21 protein on GTP hydrolysis. *Nature,* **345**, 309-315.

Shimada, T., Sasaki, N., Ohkura, R. & Sutoh, K. (1997). Alanine scanning mutagenesis of the switch I region in the ATPase site of *Dictyostelium discoideum* myosin II. *Biochemistry,* **36**, 14037-14043.

Siemankowski, R. F. & White, H. D. (1984). Kinetics of the interaction between actin, ADP, and cardiac myosin-S1. *J. Biol. Chem.* **259**, 5045-5053.

Smith, C. A. & Rayment, I. (1996a). Active site comparisons highlight structural similarities between myosin and other P-loop proteins. *Biophys. J.* **70**, 1590-1602.

Smith, C. A. & Rayment, I. (1996b). X-ray structure of the magnesium (II). ADP. vanadate complex of the *Dictyostelium discoideum* myosin motor domain to 1.9 Å resolution. *Biochemistry,* **35**, 5404-5417.

Sprang, S. R. (1997). G protein mechanisms: insights from structural analysis. *Annu. Rev. Biochem.* **66**, 639-678.

Tong, L. A., de Vos, A. M., Milburn, M. V. & Kim, S. H. (1991). Crystal structures at 2.2 A resolution of the catalytic domains of normal ras protein and an oncogenic mutant complexed with GDP. *J. Mol. Biol.* **217**, 503-516.

Uyeda, T. Q. P. & Spudich, J. A. (1993). A functional recombinant myosin II lacking a regulatory light chain-binding site. *Science,* **262**, 1867-1870.

Vale, R. D. (1996). Switches, latches, and amplifiers: common themes of G proteins and molecular motors. *J. Cell Biol.* **135**, 291-302.

Woodward, S. K. A., Eccleston, J. F. & Geeves, M. A. (1991). Kinetics of the interaction of 2′(3′)-O-(N-methylanthraniloyl)-ATP with myosin subfragment 1 and actomyosin subfragment 1: characterization of two acto-S1-ADP complexes. *Biochemistry,* **30**, 422-430.

Woodward, S. K., Geeves, M. A. & Manstein, D. J. (1995). Kinetic characterization of the catalytic domain of *Dictyostelium discoideum* myosin. *Biochemistry,* **34**, 16056-16064.

Edited by A. R. Fersht

(Received 13 April 1999; received in revised form 2 June 1999; accepted 2 June 1999)